Article

Not peer-reviewed version

The Role of Cone-Beam Computed Tomography CT Extremity Arthrography in Preoperative Assessment of Osteoarthritis

Marion Hamard , Marta Sans Merce , Karel Gorican , Pierre-Alexandre Poletti , Angeliki Neroladaki , Sana Boudabbous *

Posted Date: 23 October 2023

doi: 10.20944/preprints202310.1333.v1

Keywords: cone-beam computed tomography arthrography; X-ray; osteoarthritis; Kellgren and Lawrence classification; density; radiation

Article

The Role of Cone-Beam Computed Tomography CT Extremity Arthrography in Preoperative Assessment of Osteoarthritis

Marion Hamard *, Marta Sans Merce, Karel Gorican, Pierre-Alexandre Poletti, Angeliki Neroladaki and Sana Boudabbous [1]

Division of Radiology, Department of Diagnosis, Geneva University Hospitals, Gabrielle-Perret-Gentil 4, Geneva 1205, Geneva, Switzerland

* Correspondence: hamardmama@gmail.com

Abstract: Osteoarthritis (OA) is a prevalent disease and the leading cause of pain, disability, and quality of life deterioration. Our study sought to evaluate the image quality and dose of cone-beam computed tomography arthrography (CBCT-A) and compare them to digital radiography (DR) for OA diagnosis. Overall, 32 cases of CBCT-A and DR with OA met inclusion criteria and were prospectively analyzed. The Kellgren and Lawrence classification (KLC) stage, sclerosis, osteophytes, erosions, and mean joint width (MJW) were compared between CBCT-A and DR. Image quality was excellent in all CBCT-As, with excellent inter-observer agreement. OA under-classification was noticed with DR for MJW ($p=0.02$), osteophyte detection (<0.0001), and KLC ($P<0.0001$). The HU values obtained for the CBCT did not correspond to the values for MDCT, with a greater mean deviation obtained with the MDCT HU for MBIR1 than MBIR2. CBCT-A has been found to be more reliable for OA diagnosis than DR as revealed by our results using three-point rating scale for the qualitative image analysis, with higher quality and an acceptable dose. Moreover, the use of this imaging technique permits the preoperative assessment of extremities in OA diagnosis, the upright position and bone microarchitecture analysis being two other advantages of CBCT-A.

Keywords: cone-beam computed tomography arthrography; X-ray; osteoarthritis; Kellgren and Lawrence classification; density; radiation

1. Introduction

Osteoarthritis (OA) is a prevalent, age-related worldwide disease and the leading cause of pain, disability, and deterioration of quality of life. OA is usually defined on imaging by means of five hallmarks: joint space narrowing or mean joint width (MJW), subchondral sclerosis, marginal osteophytes, subchondral cysts (geodes), and altered shape of the joint surfaces [1]. Digital radiography (DR) remains the gold standard imaging modality for both the initial evaluation of OA and longitudinal follow-up in clinical practice and research [2–7]. It is more accessible, least expensive, and most commonly deployed imaging modality5 and allows for risk stratification [2]. Radiographic outcome measurements are still the only approved clinical trial end points by regulatory authorities [7]. DR can detect marginal osteophytes, subchondral sclerosis, and cysts, determine MJW [3–5,7]. and it is considered an established determinant of OA severity and longitudinal worsening [2]. However, it is well known that DR (uniplanar modality) is unable to directly visualize OA-associated damage in articular and periarticular non-osseous joint structures, e.g., the meniscus [2,4,5]. The smallest detectable difference of least 0.2mm average MJW of OA knee joints is observed [2].

The most widely and reliably employed semi-quantitative DR assessment for OA is the Kellgren and Lawrence classification (KLC), proposed in 1957.8 This method was initially employed to classify knee OA severity according to five grades (Table 1). As of now, this classification is widely used for all extremity OA grading: OA diagnosis is established if the score is ≥2.3 The most widely employed quantitative DR assessment is the measurement of joint MJW obtained from knee DR. These

Preprints (www.preprints.org) | NOT PEER-REVIEWED | Posted: 23 October 2023 doi:10.20944/preprints202310.1333.v1

assessments have proven reliable, in particular when they extend over a 2-year period, the radiographs obtained with the knee in a standardized flexed position [7].

Table 1. Kellegren and Lawrence classification system for osteoarthritis, as applied in this study.

Grades	Description
0	Normal, with no radiographic findings of OA
1	Doubtful joint space narrowing Doubtful osteophytes
2	Possible joint space narrowing Definite osteophytes
3	Multiple and moderately sizes osteophytes Definite joint space narrowing Small pseudocystic with sclerotic walls Possible deformity of bone contour
4	Multiple and larges osteophytes Severe joint space narrowing Marked sclerosis Definite bone deformity

OA: Osteoarthritis.

Multi-detector computed tomography (MDCT) constitutes an imaging modality with several advantages, including excellent analyses of cortical bone, soft tissue calcifications, and facet joint OA [4,5]. Furthermore, the subchondral trabecular bone architecture can be analyzed, and bone density with calcium crystal deposits be measured. The method's limitations are the radiation exposure and limited soft tissue evaluation compared with magnetic resonance imaging [5]. MDCT arthrography is the most accurate method for indirectly evaluating superficial and focal cartilage damage and other intrinsic joint structures, especially the central osteophytes that signal more severe OA changes than marginal ones alone. This method displays a high spatial resolution and high contrast between cartilage, superficial, and deep boundaries [4,5]. To resume, 3D imaging is more confident to detect earlier and precisely areas of joint loosening. Moreover, for this pre-surgical population, as you know, technique of replacement depends on involved zones and the degree of cartilage loss and CBCT directly visualize the cartilaginous surfaces. In addition, and inherent to the technique, structures are superposed for example between small bones as in carpus to detect joint narrowing mainly in sagittal plane.

Cone-beam computed tomography (CBCT), initially applied for dental imaging, has recently emerged as a new dedicated extremity imaging method. CBCT uses a pyramid-shaped DR beam and flat panel detector that rotates 216.5° around the patient. The main advantages of CBCT are its high spatial resolution [9], which permits a detailed analysis of bone architecture, lower radiation exposure, and smaller field of view (FOV) compared to MDCT [3,10]. It has been demonstrated that knee joints can now be imaged during both weight-bearing and non-weight-bearing modes, with excellent image quality for bone and good/adequate quality for soft tissues [3,11,12]. The weight-bearing (WB) mode can detect subtle evidence of joint instability [13]. We can easily assume that trabecular and cortical bone qualitative analyses are superior using CBCT than DR and that the superficial and deep cartilage analyses are preferable with CBCT arthrography (CBCT-A). In addition, the main concern of CBCT technique is the alteration of the HU with the first generation of iterative reconstruction compared with MDCT that is inherent to this modality, as further explained in the Discussion section; therefore, CBCT apparently cannot be used for estimating bone density [14]. Of note, CBCT-A is considered as an invasive method. Indeed, as a prior arthrography needs to be performed, with positive contrast medium (CM) infiltration, potential infectious and hemorrhagic complications may occur.

Preprints (www.preprints.org) | NOT PEER-REVIEWED | Posted: 23 October 2023 doi:10.20944/preprints202310.1333.v1

This study sought to better define CBCT-A's place in OA diagnosis as compared to DR, and to evaluate its clinical image quality, radiation dose, and bone density quantification for improved use of this technique in the musculoskeletal field.

2. Materials and Methods

Patient population

This prospective study was performed after cantonal ethics committee research (CCER) approval and in accordance with the guidelines of the Helsinki declaration. The number of the CCER-HUG Geneva approval is 2017-01276.

All patients were referred to our institution for CBCT (traumatology, CBCT-A, etc.) from specialized department. They were consecutively and prospectively included during seven months, during which the reconstruction station for second-generation model-based iterative reconstruction (MBIR) was available. Those patients were addressed to assess the pathological joint space in prevision of surgical intervention.

All patients provided informed consent before their participation of this study, all were aged 18 years or more.

Overall, 32 patients (men: 23; women: 9; mean age: 75.14 years) were included in the study, all referred from the orthopedic department: 18 wrist cases (two cases with both sides), nine ankle, and five knees for analysis. Two male patients underwent a CBCT-A of each wrist. All patients underwent a CBCT-A and DR of their extremity. All patient data were anonymized (SB).

Indications for the CBCT-A were assessments of OA secondary to (Figure 1): osteochondral lesion (OCL) of the talus (n= 4), osteochondritis dissecans of the talus (n=1), talocrural OA follow-up (n=1), ligamentous syndesmosis injury (n=1), after talocrural prosthesis (n=1), after debridement of OCL of talus (n=1), radio-scaphoid OA after wrist traumatism (n=7) or scaphoid fracture (n=2), after arthrodesis of carpal joint (n=1), scaphoid non-union advanced collapse (n=7), chronic instability of triangular fibrocartilage complex (n=1), knee traumatism (n=2), tibial fracture (n=1), tibial OA (n=1), and after cruciate ligament repair (n=1).

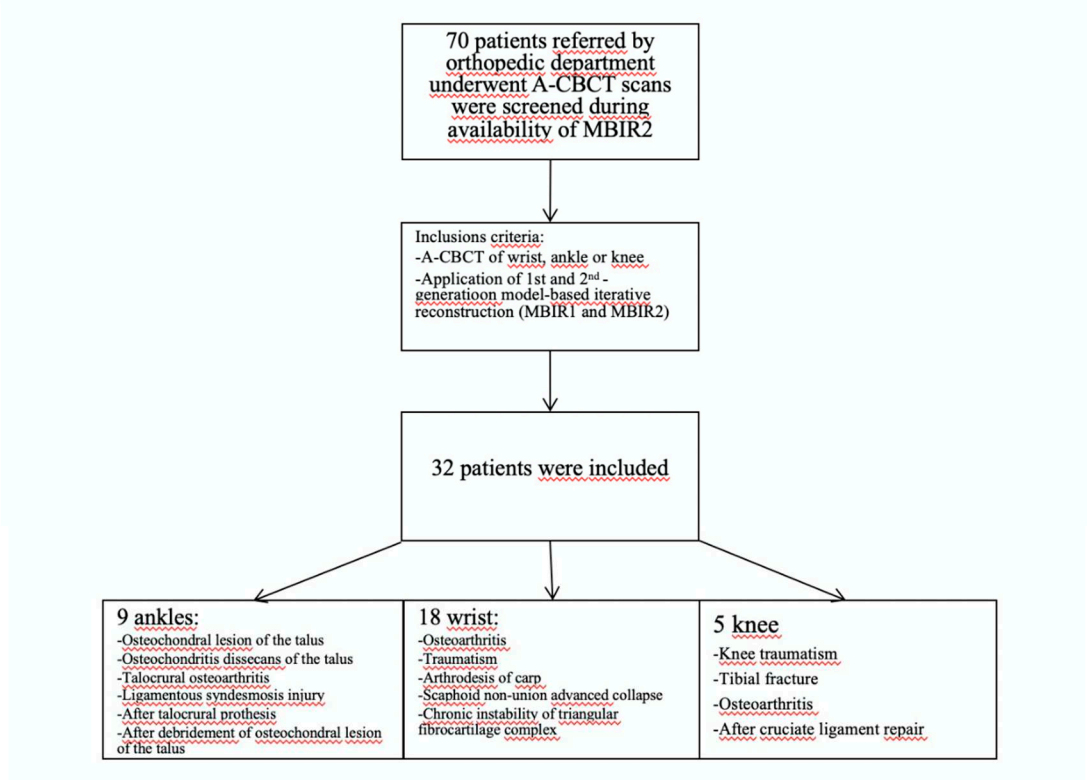

Figure 1. Diagram of patient recruitment with inclusion criteria.

Preprints (www.preprints.org) | NOT PEER-REVIEWED | Posted: 23 October 2023 doi:10.20944/preprints202310.1333.v1

DR and CBCT-A acquisition protocol and image reconstruction

An arthrography was performed 15–20 minutes before CBCT-A acquisition.

For wrist CBCT-A, we performed first percutaneous arthrography in one dedicated fluoroscopic room 20 minutes before CBCT acquisition. The patient was lying in "superman" position, with supine ventral position on the fluoroscopic table. For small joints, we used 22 G needle for articular injection of CM. We performed a mix in the syringe of 2 cc of Rapidocaine local anesthesia 1% (Sinetica SA, 200 mg/20ml) and 8cc of Iopamiron 300mg/ml (Iopaidolum 3g d'iode/10ml, Bracco Suisse SA, Switzerland). Then, we put the needle in three different localizations under fluoroscopic image-guidance, first in medio-carpal joint, second in the radio-ulnar joint, and finally in the radio-carpal joint. For ankle joint arthrography, we injected the same mix, but the patient was lying in the dorsal position on the fluoroscopic table, with leg extension, the foot on the table (plantar flexion), and ankle internal rotation of 20°. For the knee, the patient was lying in the supine position, with a flexion of 30°. The lateral approach was used to inject the CM.

In our department, the CBCT (OnSight, Carestream Health, Rochester, New York, USA) has a gantry featuring a 58cm patient aperture and movable table enabling upright position, enabling us to perform a WB CBCT for the lower extremities. The ankle and knee were scanned in the upright position (Figure 2A). The wrist was scanned with the patient sitting and the arm extended (Figure 2B). The acquisition parameters for the wrist are summarized in Table 2. Prior to the acquisition, two scouts were performed, one antero-posterior (AP) and one lateral (LAT). For more simplicity, all CBCT-A images were reconstructed in coronal and sagittal planes with the bone kernel (window width: 1500; window level: 300). All images were first reconstructed with the MBIR1 for routine practice and then reconstructed with MBIR2 in a dedicated research workstation prior to analysis [15]. All images were digitally stored in the PACS and anonymized.

Figure 2. Upright position in the WB CBCT to investigate foot, ankle or knee (**A**) and sitting position with arm extended to explore hand and wrist (**B**). WB: weight-bearing; CBCT: cone-beam computed tomography.

 doi:10.20944/preprints202310.1333.v1

Table 2. Scanning parameters of CBCT (OnSight, Carestream Health, Rochester, New York) and DR (Siemens, ISIO and Philips, DigitalDiagnost).

Parameters	CBCT	DR
Energy	80kVp	50kVp
Current	5mA	3.2mAs
FOV	216 x 216mm	
Matrix	884 x 884	
Isotropic voxel size	0.26mm	
Rotation time	25.18s	
Exposure time	21s approximately	
Scan rotation angle	216.5°	
CTDI (indicated)	3.14mGy (16cm phantom)	
Focus-detector distance		120cm

CBCT: cone-beam computed tomography; DR: digital radiography; s: second; CTDI: computed tomography dose index; DR: digital radiography.

For the radiographic technology system, we used DR. The parameters applied for DR are summarized in Table 2. For the wrist, knee, and ankle, two projections were performed, one AP and one LAT, in supine position for the knee and ankle.

Qualitative image analysis for CBCT-A

All DR and CBCT-A images were analyzed by two blinded independent MSK radiologists, one with 2 years of experience in MSK imaging and the other one with 5 years. The images were read in a dark reading room using 3D visualization software (Osirix, Rosset, Geneva, Switzerland). All CBCT-A images were analyzed for their overall quality using a three-point rating scale (2: excellent; 1: good; 0: poor).

The KLC stage was compared between the CBCT-A and DR using the usual grading score (Table 1). Erosion and sclerosis were evaluated using a three-point rating scale (0: absence; 1: density change in cortical bone; 3: density change in trabecular bone). Cartilage abnormalities were similarly evaluated using a three–point rating scale (0: normal; 1: thinning; 2: exposed subchondral bone). We used this KLC score for its simplicity. Indeed, the revised Altman atlas is more complete and more objective, but more complicated to applied in clinical routine practice [16].

Quantitative image analysis of CBCT-A

The correspondence between electronic densities and the HU was evaluated using a standardized CIRS-062MA (Norkfold, Virginia, USA) phantom (Figure 3) for the CBCT images reconstructed with the two available reconstruction algorithms: MBIR 1 and MBIR2. The results were compared to the HU obtained from the two MDCT (SOMATOM Definition Flash Siemens Healthcare and Discovery 750 HD GE Healthcare) available in our department. The phantom comprises nine inserts with different materials corresponding to different electronic densities (Figure 3A). The reproducible region of interest (ROI) (size and seat) was placed in all nine inserts (Figure 3B), with three measurements for every item. Then, we analyzed the HU for all 32 CBCT-As in the coronal plane for CM, the trabecular subchondral bone, cortical bone, and cartilage densities after application of the MBIR2. ROI were also placed in all cases, with three measurements for every item (Figure 4A). The mean was reported for statistical analysis.

Preprints (www.preprints.org) | NOT PEER-REVIEWED | Posted: 23 October 2023 doi:10.20944/preprints202310.1333.v1

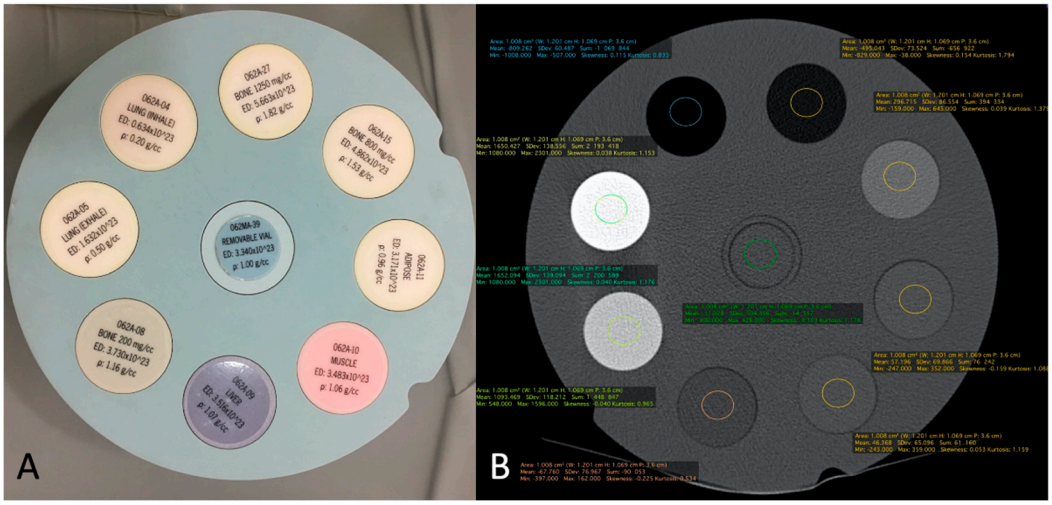

Figure 3. CIRS-062MA Phantom comprises nine inserts with different materials corresponding to different electronic densities (A). It is used to calibrate the system in terms of HU for eight different electronic densities corresponding to 8 tissues and a standard removable vial for CBCT and MDCT. Example of ROI measurement of each density tunnel (B). HU: Hounsfield unit; CBCT: cone-beam computed tomography; MDCT: multi-detector computed tomography; ROI: region of interest.

Finally, MJWs were calculated, of the lateral and medial sides for the knee and center of the radio-carpal joint in the wrist or talocrural joint in the ankle, the tibio-talar joint in the ankle, and the femoro-tibial joint in the knee (Figure 4B) and compared with the corresponding DR images.

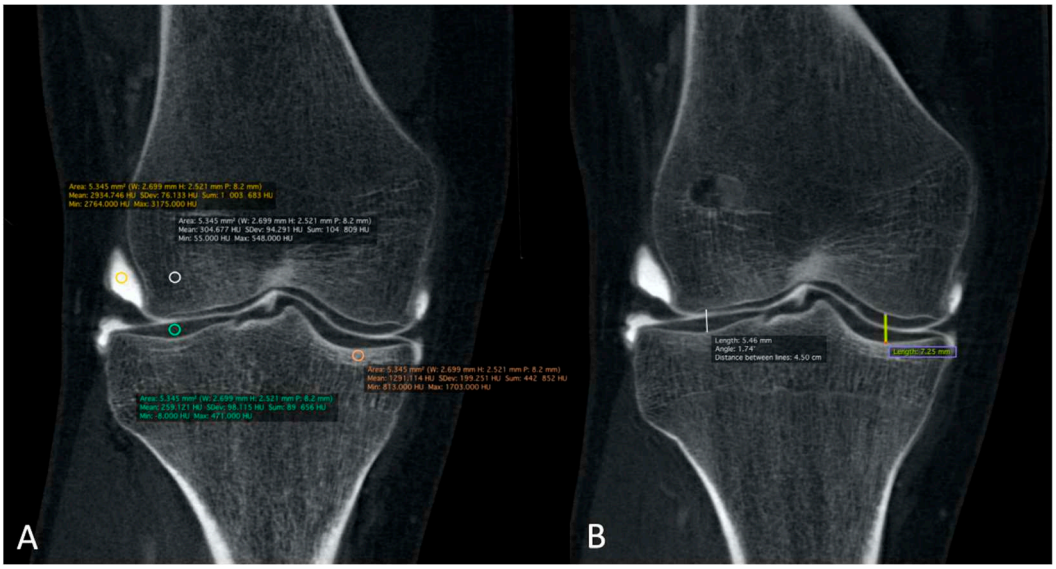

Figure 4. The HU numbers and JSN of all 32 CBCT-As were analyzed in coronal plane after application of MBIR2. Here, example of a right knee is shown. HU for CM, trabecular and cortical sub chondral bone and for cartilage densities were reported. ROI were also placed with three measurements for every item (A). The MJW was evaluated with the MJW at the lateral and medial side of the femoro-tibial joint (B). HU: Hounsfield unit; CBCT-A: cone-beam computed tomography arthrography; ROI: region of interest; MJW: mean joint width. HU: Hounsfield unit; CBCT: cone-beam computed tomography; MDCT: multi-detector computed tomography; ROI: region of interest.

Radiation dose measurement of DR and CBCT-A

To evaluate the radiation exposure for the CBCT-A compared to the DR, a polymethylmethacrylate (PMMA) phantom with dimensions of 20x15x4cm3 (Figure 5) was used to simulate the hand and wrist. Doses to the hand and wrist were estimated by measuring the absorbed

 doi:10.20944/preprints202310.1333.v1

dose using a 10cm cylindrical ionization chamber placed at the center of the PMMA phantom. The absorbed dose was measured for the two scouts (PA, LAT) + one 3D acquisition of the CBCT-A and for the two views (AP+LAT) of the conventional DR.

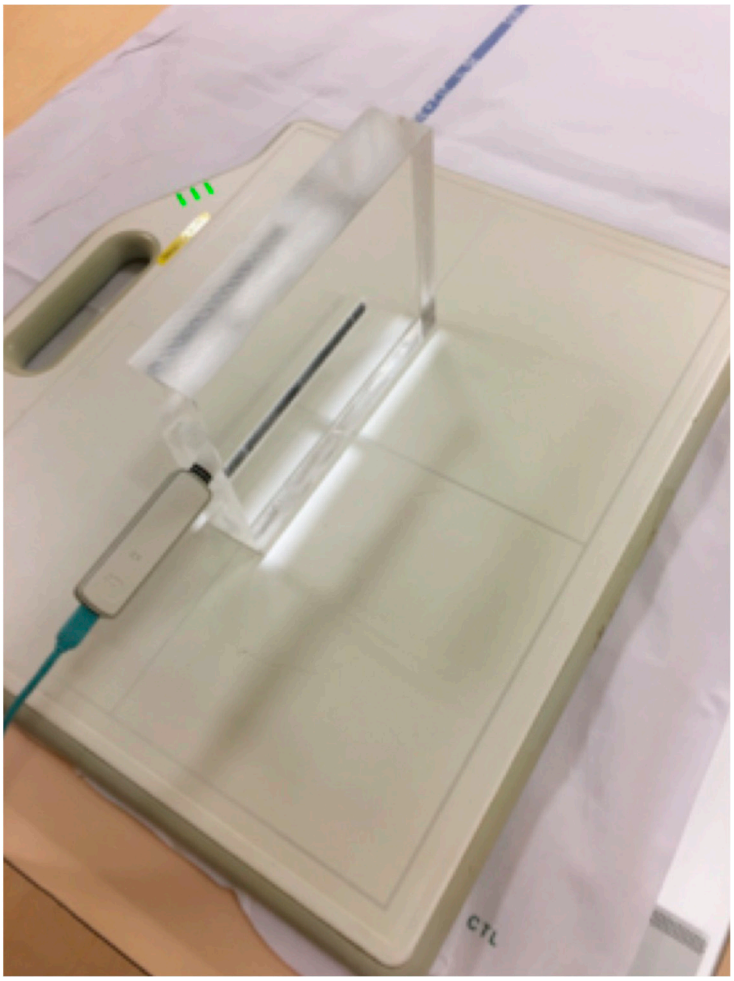

Figure 5. Plexiglas phantom (PMMA) used to represent hand or wrist extremities to calculate absorbed dose of CBCT and DR imaging modalities, with dimensions of 20x15x4cm^3 (A). CBCT: cone-beam computed tomography; DR: digital radiography.

No effective dose information could be computed based on our measurements. Nevertheless, measurement of absorbed doses at the center of the phantom remains a valid method for comparing the exposure between the two different modalities [17].

Statistical analysis

First, for qualitative analysis and to compare image quality of CBCT-A by the two readers, we used Kappa coefficient. Interpretation of agreement statistic scores between the two readers for DR and A-CBCT concerning erosions, sclerosis, MJW and KLC was carried out using criteria developed by Landis and Koch. Values of 0-0.20 represent slight agreement, 0.21-0.40 fair agreement, 0.41-0.60 moderate agreement, 0.61-0.80 substantial agreement, 0.81-1 is considered almost perfect agreement [18]. Furthermore, we compared DR with A-CBCT concerning the qualitative assessment for erosions, sclerosis, and quantitative measurements of MJW, as well as KLC for DR and A- CBCT-A using Prism software (Graphic Pad Prism Version 6.0e). Column analyses using t-test were performed. Owing to the non-Gaussian distribution, the Wilcoxon matched pairs signed rank test was employed to compare the results. P value <0.05 was considered statistically significant.

Preprints (www.preprints.org) | NOT PEER-REVIEWED | Posted: 23 October 2023 doi:10.20944/preprints202310.1333.v1

3. Results

The qualitative image analysis was excellent in all CBCT-A cases, with an excellent inter-observer concordance (kappa=1), as shown in Figures 4 and 6. Twenty-four patients had an OA diagnosis (KLC ≥2) with the CBCT-A, and twenty-one were subclassed with DR. No statistically significant difference was observed in terms of sclerosis (p=0.29) and erosion (p=0.184) between both modalities. Examples of OA underestimation, with DR compared with CBCT-A are shown in Figure 6.

Figure 6. CBCT-A of left wrist in coronal (A) and sagittal (B) planes, that showed subchondral erosion (A; white arrow) and definite anterior osteophyte of radial lip with MJW (B; red arrow), Grade 3 of KLC scoring system. The AP DR showed a possible joint space narrowing between scaphoid and radial styloid (C; dark dotted circle), grade 2 of KLC scoring system. The KL grading on XR under estimated compared to CBCT-A. CBCT-A: cone-beam computed tomography arthrography; MJW: mean joint width; AP DR: antero-posterior digital radiography; KLC: Kellegren and Lawrence classification

Concerning the quantitative image analysis, OA under-classification was noticed with DR regarding MJW (p=0.02), detection of osteophytes (<0.0001), and KLC (P<0.0001), as shown in Table 3.

Table 3. P values of CBCT criteria in OA grading compared with DR.

	Median	Rs (Spearman)	P values
Mean joint width (MJW)	0.09876	0.9405	0.0213
Kellegren and Lawrence	-1.000	0.6350	<0.0001
Osteophytes	0.0	0.4848	<0.0001

Preprints (www.preprints.org) | NOT PEER-REVIEWED | Posted: 23 October 2023 doi:10.20944/preprints202310.1333.v1

Subchondral sclerosis	0.0	0.3551	0.2972
Erosions	0.0	0.3393	0.1849

CBCT: cone-beam computed tomography; OA: osteoarthritis; DR: digital radiography.

Table 4 summarizes the results obtained from the calibration of the HU with the standardized phantom. Measurements in both the MDCT (Siemens and GE) revealed similar densities in all tissues analyzed. For CBCT, the HU did not correspond to the usual values obtained for the MDCT, with a greater mean deviation obtained with the CT HU for the MBIR1 than MBIR2. The mean HU calculated for the CBCT-A was 1966 for CM, 328 for trabecular bone, 812 for subchondral cortex, and 330 for cartilage. We focused on bone density, as no normal values were found in the literature for cartilage; regarding CM, the contrast was diluted with the joint effusion in many cases. We noticed that the HU of CBCT-A measured for trabecular bone and cartilage were similar and correspondeded to the bone density values of 200mg/cc for the MDCT, with either MBIR1 or MBIR2 (236-298HU). The HU of subchondral cortical bone on CBCT-A was similar to the HU of bone with a density of 80mg/cc on MDCT, particularly with MBIR2 (Table 4).

Table 4. Mean density values in HU from MDCT (Siemens and GE) and CBCT with MBIR1 and MBIR2.

	GE CT densities	**Siemens MDCT densities**	**CBCT with MBIR 1 densities**	**CBCT with MBIR2 densities**
Bone of 1250 mg/cc (ρ :1.82 g/cc)	1651.115 (SD: 149.550)	1652.094 (SD: 139.094)	1895.378 (SD: 142.514)	1061 (SD: 97.320)
Bone of 800 mg/cc (ρ :1.53g/cc)	1091.529 (SD: 93.369)	1093.469 (SD: 118.212)	1282.889 (SD: 118.033)	858.058 (SD: 85.509)
Bone of 200 mg/cc (ρ :1.16 g/cc)	298.070 (SD: 78.129)	296.715 (SD: 73.)	298.396 (SD: 78.129)	236.401 (SD: 59.354)
Adipose tissue (ρ :0.96 g/cc)	-68.434 (SD: 77.762)	-67.760 (SD: 76.967)	-73.072 (SD: 71.203)	-70.934 (SD: 62.959)
Muscle (ρ :1.06 g/cc)	43.208 (SD: 68.922)	46.368 (SD: 65.096)	33.949 (SD: 74.198)	15.139 (SD: 57.353)
Liver (ρ :1.07 g/cc)	56.396 (SD: 76.148)	57.196 (SD: 69.866)	42.652 (SD: 75.826)	26.372 (SD: 55.516)
Lung (inhale) (ρ :0.20 g/cc)	-810.597 (SD: 67.894)	-809.262 (SD: 60.487)	-862.192 (SD: 52.165)	-760.330 (SD: 59.773)
Lung (exhale) (ρ :0.50 g/cc)	-493.688 (SD: 79.298)	-495.043 (SD: 73.524)	-560.997 (SD: 57.972)	-494-122 (SD: 56.538)

MDCT: multi-detector computed tomography; CBCT: cone-beam computed tomography; s: second; SD: standard deviation; MBIR: model-based iterative reconstruction.

The absorbed dose to the hand-wrist for the CBCT-A was estimated higher than that of the DR; results for the absorbed doses have been presented in Table 5.

 doi:10.20944/preprints202310.1333.v1

Table 5. Absorbed dose measured with the PMMA phantom for CBCT-A and DR.

	CBCT-A	DR
Dose radiation for PA projection mGy	0.037mGy	0.029mGy
Dose radiation for oblique/lateral projection	0.013mGy	0.033mGy
1 3D acquisition	4.902mGy	--
Total dose radiation	4.952mGy	0.062mGy

CBCT-A: cone-beam computed tomography; DR: digital radiography; s: second.

4. Discussion

In our study, we have highlighted that the image quality was excellent in all cases of the CBCT-A study. These results are consistent with those from previous studies [9,19], with excellent visualization of bone microarchitecture, primarily due to the high spatial resolution of this technique [2,9,11,12,19,20]. To the best of our knowledge, this study is the first to demonstrate the advantages of using the CBCT-A scan for the grading of OA, as it permits a better treatment. Even though the DR remains the imaging modality of choice in the initial investigation of OA [2–5,7], CBCT-A offers many advantages in investigating OA. It provides superior diagnostic performance and staging for cartilage lesions, as shown in the study of Posadzy et al. [19], with better KLC scoring of OA despite its invasiveness. Furthermore, it allows for a better visualization of cartilage, for this structure is non-radiopaque, and of other intrinsic joint structures, especially in the knee joint (e.g., the meniscus). Penetration of CM within deeper layers of the cartilage surface indicates an articular-sided defect of chondral surface [4]. In the study by Carrino et al. [9], the authors were limited by the presence of artifacts, for which no artifact correction algorithm was applied in the first CBCT generation. These artifacts were clearly diminished in our recent device, mostly due to the new iterative reconstruction algorithm installed with MBIR2 rather than with MBIR1. In our study, we also observed that there was an OA under-classification when using DR regarding MJW, detection of osteophytes, and KLC.

Other clinical advantages of this device were revealed as well. As mentioned in other studies, CBCT allows for the WB investigation of extremities [2,9,11,12,19–23] which still needs to be further studied. Furthermore, the three-dimensional data of CBCT facilitate more quantitative analyses, such as segmentation, erosion detection, characterization of subchondral bone architecture, and measurement of bone mineral density [9].

For CBCT, the HU did not correspond to the usual values obtained for the MDCT, with a mean deviation from the CT HU larger with the MBIR1 at -72% (SSD 221) than the MBIR2 at -52% (SSD 94). The current study is the first to compare these HU values between the MDCT and CBCT with two different iterative reconstruction algorithms: MBIR1 and MBIR2. The better results found with the MBIR2 were probably due to the device progress in the iterative reconstruction algorithm. Several studies have concluded that CBCT cannot be used for quantification purposes due to the poor calibration in the HU [14]. Swennen et al. stated that with CBCT, the "HU" of an organ's voxel depends on the position in the image volume [24]. This means that DR attenuation of CBCT acquisition systems changes according to the position, producing different HU values for similar bony or soft tissue structures in different areas of the scanned volume. The partial gantry rotation causes an asymmetric dose distribution in the anatomical region of interest [17,25,26]. As seen in this study, the HU were getting closer to the usual values obtained for the MDCT with MBIR2 as compared to MBIR1 (mean deviation from the CT HU of -72% for MBIR1 and -52% for MBIR2). Thus, we can expect that further improvement in cone-beam reconstruction algorithms and post-processing will reduce this drawback, permitting to obtain HU closer to those of the MDCT, thereby enabling quantitative measurements of some diseases, such as bone necrosis and osteopenia follow-ups.

Concerning the radiation dose, CBCT delivers an absorbed dose (AD) that is higher than that delivered by one DR examination (4.92mGy and 0.062mGy respectively), the AD of 4.952mGy obtained for the CBCT in our study comparing well with that obtained for the Planmed Verity CBCT

 doi:10.20944/preprints202310.1333.v1

in the Koivisto et al. study [17]. Indeed, the absorbed dose in Koivisto et al.'s study was evaluated at 1.99mGy using an anthropomorphic RANDO wrist phantom. Doses to the different tissues were measured, and an average AD was computed. Their device installation worked at approximately the same kVp as our device but with 36mAs per acquisition compared to our device's 105mAs. Together with the different method of evaluating AD, the different mAs used for each system could partly explain why the AD in our study was approximately 2.5 times higher than theirs. Concerning the AD for the conventional AP + LAT XR, the Koivisto et al.'s study presented a value of 850 Gy compared to that obtained in our study of 62 Gy. Again, the main difference originates from the mAs used in each case, kVp, and difference in the measurement methodology.

This study displays several limitations. First, we included only a small number of patients given that the CBCT-A scan still displays limited indications, and this technique is only requested by specialized orthopedists, mainly consisting of hand and foot-ankle surgeons. Despite our group's heterogeneity, including wrists, ankles, and knees, this preliminary study primarily sought to position CBCT-A as a technique for the preoperative OA management. Based on our data, CBCT-A could be a technique enabling several joint analyses.

The lack of an HU standard on CBCT systems is another drawback. We, however, believe that improvements with new devices and reconstruction algorithms will allow for a better assessment of bone density and crucial point prosthetic surgery.

The dose comparison among the different modalities can be performed by assessing the measured absorbed doses [21], though authors are aware that it is common and widely accepted to compare exposures from different modalities while using the effective dose. At present, nevertheless, there are not any readily available methods to evaluate the effective dose (ED) from a hand or wrist examination, i.e., conversion factors from absorbed doses to effective doses for DR or CBCT examinations. The evaluation of the ED could be performed through measuring the organ absorbed doses in the wrist area by inserting dosimeters in a custom-made anthropomorphic RANDO wrist phantom, as performed by Koivisto et al [21–24].

5. Conclusions

In conclusion, the CBCT-A is more reliable for OA diagnosis than DR as revealed in our results using three-point rating scale for the qualitative image analysis, with higher quality and an acceptable dose. We entirely agree that the dose comparison by means of mGy (CT dose index) provides the impression of significant doses being used on CBCT. However, we would like to remind the reader that doses by DR techniques prove to be insignificant, the effective dose in mSv being significantly lower, as the conversion factor for extremities is very low.

Furthermore, the use of this imaging technique permits mainly the preoperative assessment for extremities in OA diagnosis, the upright position and the bone microarchitecture analysis are two other advantages of CBCT-A.

Author Contributions: Conceptualization and methodology: Sana Boudabbous, Marta Sans Merce, Marion Hamard; Formal analysis: Sana Boudabbous, Marta Sans Merce, Karel Gorican, Angeliki Neroladaki; Investigation: Sana Boudabbous, Marta Sans Merce, Karel Gorican, Angeliki Neroladaki; Writing—original draft preparation: Marion Hamard, Sana Boudabbous, Marta Sans Merce; Review: Marion Hamard, Sana Boudabbous, Marta Sans Merce, Karel Gorican, Angeliki Neroladaki, Pierre-Alexandre Poletti; Editing: Marion Hamard, Sana Boudabbous, Marta Sans Merce; Visualization: Marion Hamard, Sana Boudabbous, Marta Sans Merce; Project administration: Marion Hamard, Sana Boudabbous; All authors have read and agreed to the published version of the manuscript.

Funding: This research received no external funding.

Institutional Review Board Statement: Not applicable.

Informed Consent Statement: Informed consent was obtained from all subjects involved in the study.

Data Availability Statement: The data presented in this study are available on request from the corresponding author.

Conflicts of Interest: The authors declare no conflict of interest.

References

1. Jacobson JA, Girish G, Jiang Y, Sabb BJ. Radiographic evaluation of arthritis: degenerative joint disease and variations. *Radiology* **2008**, 248, 737–747. doi: 10.1148/radiol.2483062112.
2. Demehri S, Guermazi A, Kwoh CK. Diagnosis and Longitudinal Assessment of Osteoarthritis: Review of Available Imaging Techniques. *Rheum Dis Clin North Am*. **2016**, 42, 607–620. doi: 10.1016/j.rdc.2016.07.004.
3. Demehri S, Hafezi-Nejad N, Carrino JA. Conventional and novel imaging modalities in osteoarthritis: current state of the evidence. *Curr Opin Rheumatol.* **2015**, 27, 295–303. doi: 10.1097/BOR.0000000000000163.
4. Hayashi D, Guermazi A, Crema MD, Roemer FW. Imaging in osteoarthritis: what have we learned and where are we going? *Minerva Med*. **2011**, 102, 15–32.
5. Hayashi D, Roemer FW, Guermazi A. Imaging for osteoarthritis. *Ann Phys Rehabil Med*. **2016**, 59, 161–169. doi: 10.1016/j.rehab.2015.12.003.
6. Liang X, Liu S, Qu X, Wang Z, Zheng J, Xie X, Ma G, Zhang Z, Ma X. Evaluation of trabecular structure changes in osteoarthritis of the temporomandibular joint with cone beam computed tomography imaging. *Oral Surg Oral Med Oral Pathol Oral Radiol*. **2017**, 124, 315-322. doi: 10.1016/j.oooo.2017.05.514.
7. Roemer FW, Eckstein F, Hayashi D, Guermazi A. The role of imaging in osteoarthritis. *Best Pract Res Clin Rheumatol.* **2014**, 28, 31–60. doi: 10.1016/j.berh.2014.02.002.
8. Kellgren JH, Lawrence JS. Radiological assessment of osteo-arthrosis. *Ann Rheum Dis*. **1957**, 16, 494–502. doi: 10.1136/ard.16.4.494.
9. Carrino JA, Al Muhit A, Zbijewski W, Thawait GK, Stayman JW, Packard N, Senn R, Yang D, Foos DH, Yorkston J, et al. Dedicated cone-beam CT system for extremity imaging. *Radiology* **2014**, 270, 816-824. doi: 10.1148/radiol.13130225.
10. Cao Q, Thawait G, Gang GJ, Zbijewski W, Reigel T, Brown T, Corner B, Demehri S, Siewerdsen JH. Characterization of 3D joint space morphology using an electrostatic model (with application to osteoarthritis). *Phys Med Biol*. **2015**, 60, 947-960. doi: 10.1088/0031-9155/60/3/947.
11. Prakash P, Zbijewski W, Gang GJ, Ding Y, Stayman JW, Yorkston J, Carrino JA, Siewerdsen JH. Task-based modeling and optimization of a cone-beam CT scanner for musculoskeletal imaging. *Med Phys*. **2011**, 38, 5612-5629. doi: 10.1118/1.3633937.
12. Zbijewski W, De Jean P, Prakash P, Ding Y, Stayman JW, Packard N, Senn R, Yang D, Yorkston J, Machado A, et al. A dedicated cone-beam CT system for musculoskeletal extremities imaging: design, optimization, and initial performance characterization. *Med Phys*. 2011, 38, 4700-4713. doi: 10.1118/1.3611039.
13. Sharma L, Eckstein F, Song J, Guermazi A, Prasad P, Kapoor D, Cahue S, Marshall M, Hudelmaier M, Dunlop D. Relationship of meniscal damage, meniscal extrusion, malalignment, and joint laxity to subsequent cartilage loss in osteoarthritic knees. *Arthritis Rheum*. **2008**, 58, 1716-1726. doi: 10.1002/art.23462.
14. De Vos W, Casselman J, Swennen GR. Cone-beam computerized tomography (CBCT) imaging of the oral and maxillofacial region: a systematic review of the literature. *Int J Oral Maxillofac Surg*. **2009**, 38, 609–625. doi: 10.1016/j.ijom.2009.02.028.
15. Boudabbous S, Arditi D, Paulin E, Syrogiannopoulou A, Becker C, Montet X. Model-Based Iterative Reconstruction (MBIR) for the Reduction of Metal Artifacts on CT. *AJR Am J Roentgenol*. **2015**, 205, 380–385. doi: 10.2214/AJR.14.13334.
16. Altman RD, Gold GE. Atlas of individual radiographic features in osteoarthritis, revised. *Osteoarthritis Cartilage 2007*, 15 Suppl A, A1–56. doi: 10.1016/j.joca.2006.11.009.
17. Koivisto J, van Eijnatten M, Kiljunen T, Shi XQ, Wolff J. Effective Radiation Dose in the Wrist Resulting from a Radiographic Device, Two CBCT Devices and One MSCT Device: A Comparative Study. *Radiat Prot Dosimetry* **2018**, 179, 58–68. doi: 10.1093/rpd/ncx210.
18. Koch GG, Landis JR, Freeman JL, Freeman DH, Lehnen RG. General Methodology for Analysis of Experiments with Repeated Measurement of Categorical Data. *Biometrics* **1977**, 33, 133–158.
19. Posadzy M, Desimpel J, Vanhoenacker F. Cone beam CT of the musculoskeletal system: clinical applications. *Insights Imaging* **2018**, 9, 35–45. doi: 10.1007/s13244-017-0582-1.
20. Koskinen SK, Haapamäki VV, Salo J, Lindfors NC, Kortesniemi M, Seppälä L, Mattila KT. CT arthrography of the wrist using a novel, mobile, dedicated extremity cone-beam CT (CBCT). *Skeletal Radiol*. **2013**, 42, 649-657. doi: 10.1007/s00256-012-1516-0.
21. Huang AJ, Chang CY, Thomas BJ, MacMahon PJ, Palmer WE. Using cone-beam CT as a low-dose 3D imaging technique for the extremities: initial experience in 50 subjects. *Skeletal Radiol*. 2015, 44, 797-809. doi: 10.1007/s00256-015-2105-9.
22. Kokkonen HT, Suomalainen JS, Joukainen A, Kröger H, Sirola J, Jurvelin JS, Salo J, Töyräs J. In vivo diagnostics of human knee cartilage lesions using delayed CBCT arthrography. *J Orthop Res*. **2014**, 32, 403-412. doi: 10.1002/jor.22521.
23. Mys K, Stockmans F, Vereecke E, van Lenthe GH. Quantification of bone microstructure in the wrist using cone-beam computed tomography. *Bone* **2018**, 114, 206–214. doi: 10.1016/j.bone.2018.06.006.
24. Swennen GR, Schutyser F. Three-dimensional cephalometry: spiral multi-slice vs cone-beam computed tomography. *Am J Orthod Dentofacial Orthop*. **2006**, 130, 410–416. doi: 10.1016/j.ajodo.2005.11.035.

25. Koivisto J, Kiljunen T, Kadesjo N, Shi XQ, Wolff J. Effective radiation dose of a MSCT, two CBCT and one conventional radiography device in the ankle region. *J Foot Ankle Res.* **2015**, 8, 8. doi: 10.1186/s13047-015-0067-8.
26. Koivisto J, Kiljunen T, Wolff J, Kortesniemi M. Assessment of effective radiation dose of an extremity CBCT, MSCT and conventional X ray for knee area using MOSFET dosemeters. *Radiat Prot Dosimetry* **2013**, 157, 515–524. doi: 10.1093/rpd/nct162.